RESEARCH

Coronal Signatures of Flare Generated Fast-Mode Wave at EUV and Radio Wavelengths

V. Vasanth[1]

Abstract

This paper presents a detailed study of the type II solar radio burst that occurred on 06 March 2014 using combined data analysis. It is a classical radio event consisting of type III radio burst and a following type II radio burst in the dynamic spectrum. The type II radio burst is observed between $235 - 130$ MHz ($120 - 60$ MHz) in harmonic (fundamental) bands with the life time of 5 minutes between $09:26 - 09:31$ UT. The estimated speed of type II burst by applying two-fold Saito model is ~ 650 km s^{-1}. An extreme ultraviolet (EUV) wave is observed with Atmospheric Imaging Assembly (AIA) onboard the Solar Dynamics Observatory (SDO). The very close temporal onset association of the EUV wave and flare energy release indicates that the EUV wave is likely produced by a flare pressure pulse. The eruption is also accompanied by a weak coronal mass ejection (CME) observed with the coronagraphs onboard the Solar and Heliospheric Observatory (SOHO) and the twin Solar Terrestrial Relations Observatory (STEREO). The plane of sky speed of the CME was ~ 252 km s^{-1} in the SOHO/LASCO-C2 and ~ 280 km s^{-1} in the STEREO-B/SECCHI-COR1 images. The EUV wave has two wave fronts, one expanding radially outward and the other one moving along the flare loop arcade. The source position of the type II burst imaged by the Nançay Radio Heliograph (NRH) shows that it was associated with the outward moving EUV wave. The CME is independent of the shock wave as confirmed by the location of NRH radio sources below the CME's leading edge. Therefore the type II radio burst is probably ignited by the flare. This study shows the possibility of EUV wave and coronal shock triggered by flare pressure pulse, generating the observed type II radio burst.

Keywords Type II radio bursts · Flares · Coronal mass ejections (CMEs) · Shocks

1. Introduction

The coronal disturbances and shock waves are formed during the energy release processes such as flares and coronal mass ejections (CMEs). Both CMEs and solar flares are efficient in accelerating electrons and producing shock waves whose radio signatures in the dynamic spectra are called solar type II radio bursts (McLean and Labrum, 1985; Dulk, 1985;

✉ V. Vasanth
  vasanth.veluchamy@uj.edu.pl

1   Astronomical Observatory of Jagiellonian University, Krakow 30-244, Poland

🖄 Springer

Reames, 1999; Vršnak and Cliver, 2008; Kong et al., 2012; Feng et al., 2013; Chen et al., 2014). Type II radio bursts are the earliest known signature of shock waves, drifting from high to low frequency in the dynamic spectrum due to emission at the local plasma frequency and/or its harmonics generated via plasma emission mechanism (Payne-Scott, Yabsley, and Bolton, 1947; Wild and McCready, 1950; Nelson and Melrose, 1985). The coronal type II burst generally occurs at the frequency range of $300 - 20$ MHz corresponding to the height of $1.3 - 3$ $R_{\odot}$. The interplanetary type II bursts at decametric, hectometric, and kilometric wavelengths occur at the frequency range of 14 MHz $- 20$ kHz generally beyond 2 $R_{\odot}$ and are known to be driven by fast and wide CMEs (Gopalswamy et al., 2001; Lara et al., 2003; Vasanth and Umapathy, 2013a,b; Prakash et al., 2012; Shanmugaraju et al., 2018). IP type II bursts recorded at large heliocentric distances can be considered as a possible remote sensing indicator for forecasting space weather effects (Gopalswamy et al., 2001; Vasanth et al., 2015).

Solar flares, CMEs, and shock waves are closely associated with one another, and their association rate increases with the flare importance (Vršnak and Cliver, 2008). Also, there is a good synchronization between CME acceleration and impulsive phase of flares (Zhang et al., 2001, 2004; Vršnak et al., 2004; Maričić et al., 2007; Temmer et al., 2010). Due to this, it is often difficult to identify the origin of coronal shocks, i.e., to distinguish whether they are ignited by a flare or initiated by a CME. In recent years, a number of case studies have shown that coronal shocks are driven by CMEs. However, there are cases of type II bursts observed in the absence of CMEs or associated with slow CMEs, which indicate that they might be generated by flare blast waves (Vršnak and Lulić, 2000; Vršnak, 2001; Vršnak and Cliver, 2008; Magdalenić et al., 2008, 2010, 2012; Vasanth et al., 2011, 2014; Kumar et al., 2013; Kumar, Innes, and Cho, 2016).

Solar eruptions are frequently accompanied by large-scale coronal wave phenomena known as EUV wave, first observed by the Extreme-ultraviolet Imaging Telescope (EIT) onboard the SOHO spacecraft (Thompson et al., 1999). Some reports using SOHO/EIT images claim that EUV waves are related to pressure pulse of a flare (Wu et al., 2001; Vršnak et al., 2002; Vršnak and Cliver, 2008). The shock waves of such events are generally associated with impulsive flares of short duration. On the other hand, a number of studies argue that weak flares cannot induce large-scale waves, which indicates that EUV waves are caused by CMEs. Even now the source of EUV wave is under debate (Long et al., 2017).

The previous studies had reported that the CMEs propagating with speed < 400 km s^{-1} are not likely to produce the coronal shocks. However, Pohjolainen and Lehtinen (2006) found evidence that flare-related CME acceleration can excite type II bursts even if the CME remains slow. Apparently, local conditions have to be favorable for the shock formation, one of which is certainly low Alfvénic speed.

This paper presents a case study of the metric type II burst observed on 06 March 2014. This event was previously analyzed by Kumar and Innes (2015) using SDO/AIA field of view (FOV), and concluded that a fast-mode EUV wave was generated by flare pressure pulse, which excited metric type II burst. The present paper will focus on the context of radio observations and their relations to solar eruptions. The fact is that a CME was recorded in the STEREO/SECCHI and SOHO/LASCO FOV, was not discussed in the previous study. Therefore the relationship between the type II burst, EUV wave, and CME structure will be explored in detail using Nançay Radio Heliograph (NRH) observations.

2. Observations

The dynamic spectrum of the type II radio burst was recorded on 06 March 2014 by the OR-FEES radio spectrograph from $500 - 144$ MHz and the Learmonth from $180 - 25$ MHz. The
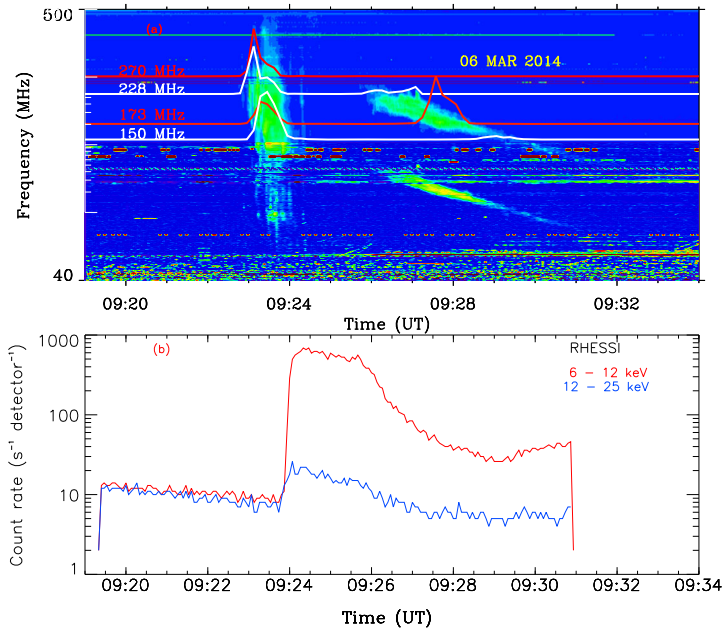
Figure 1 (a) Combined radio dynamic spectrum recorded by ORFEES (500 – 144 MHz) and Learmonth (180 – 25 MHz). Both the fundamental and harmonic components of the type II burst are clearly observed between 09:26 UT and 09:31 UT. The red lines (red labels) represent the total flux at 270 and 173 MHz, and white lines (white labels) represent the total radio flux at 228 and 150 MHz obtained by NRH observations; (b) RHESSI X-ray profile in two energy bands at 6 – 12 and 12 – 25 keV.

composite of the spectral data is presented in Figure 1a. The burst showed fundamental and harmonic emissions, both well observed with duration of 5 minutes between 09:26 – 09:31 UT. Two minutes before the type II burst, a type III radio burst was also recorded and shown in Figure 1a. The type II appears only in the metric domain, i.e., no longer wavelength type II radio burst was recorded by Wind/WAVES (Bougeret et al., 1995) and STEREO-B/WAVES (Bougeret et al., 2008).

This study uses radio imaging from the NRH at selected frequencies 408, 327, 298, 270, 228, 173 and 150 MHz (Kerdraon and Delouis, 1997). The spatial resolution of NRH images depends on the imaging frequency and observational time, being $1' - 3'$ at 327 MHz, decreasing to $3' - 6'$ at 150 MHz. The highest temporal resolution of NRH is 0.25 s resolution. The present study utilized the data with 0.25-s resolution and integrated them to 1 s.

The type II radio burst is associated with a solar eruption from the NOAA active region (AR11998) at the south-eastern limb. The eruption is accompanied by a compact or small flare located around S07E64, which starts at 09:23 UT, peaks at 09:25 UT, and ends at 09:30 UT according to the Reuven Ramaty High-Energy Solar Spectroscopic Imager (RHESSI) hard X-ray data (Lin et al., 2002) (see Figure 1). There is no GOES soft X-ray flare observation available during the time. The accompanying CME is observed by several instruments at various EUV wavelengths from the inner to outer corona and with coronagraphs in white light (WL). These instruments include AIA (Lemen et al., 2012) onboard SDO, which records the full disk image of the Sun with a cadence of 12 s (Pesnell, Thompson, and Chamberlin, 2012) and the EUV Imagers (EUVI) onboard STEREO/SECCHI with one ahead and the other behind the Earth separated by ~ 46 degrees (Kaiser et al., 2008),

The longitudinal position of STEREO-A and -B with respect to the Earth are -161 and 153 degrees, making a separation of ~ 46 degrees. Both A and B were near the far side of the Sun. The observed eruption is a south-eastern limb event in the Sun [SDO/AIA and SOHO/LASCO FOV] and is observed only by STEREO-B and not by STEREO-A. At larger heights the CME is observed by the Large Angle Spectrometric Coronagraph (LASCO) C2 (Brueckner et al., 1995) onboard the SOHO spacecraft (Domingo, Fleck, and Poland, 1995). The observed CME structure is diffuse in SDO/AIA FOV but is clear and well observed in STEREO-B/SECCHI-COR1 and SOHO/LASCO-C2 images (Figure 3). The speed of the CMEs was estimated as ~ 252 km s^{-1} in the SOHO/LASCO-C2 and ~ 280 km s^{-1} in the STEREO-B/SECCHI-COR1 FOV.

3. Data-Analysis and Results

3.1. Solar Radio Emission and EUV-White Light Eruptive Structures

The type II solar radio burst in the dynamic spectrum [Figure 1a] shows the drifting feature in both the fundamental ($120 - 60$ MHz) and harmonic bands ($235 - 135$ MHz). It is well established by the earlier reports that in meter wavelength radio emission the harmonic band is more intense and better defined than the fundamental one (Vršnak, 2001). Using $2\times$ Saito electron density model (Saito et al., 1970), the height of the type II burst is estimated by selecting several points from the harmonic band, and then they are converted into fundamental for further estimations. The estimated heights are shown in the height–time plot in Figure 6. The estimated speed of type II burst is ~ 650 km s^{-1}.

The type II burst is found to be accompanied by a compact flare located at S07E64 by RHESSI observations (Figure 1). It further confirms the presence of non-thermal electrons at flare timing. There is a weak CME associated with this eruption but not reported in the previous study by Kumar and Innes (2015).

The EUV images showed a fast-propagating wave, probably the shock wave, which moved outward and could have generated the type II burst. The EUV wave is very clearly observed in the AIA 171 Å channel, and the base difference images were used to determine the kinematics and propagation speed using slice-cut between $09:23 - 09:26$ UT. The estimated mean speed of the wave is ~ 820 km s^{-1}, obtained by linear fit to the selected data points in the interval. Both the flare energy release and onset of EUV wave occurred simultaneously around 09:23 UT (see Kumar and Innes (2015) for details). Therefore the wave is most likely generated by the flare pressure pulse. The EUV wave at AIA 171 Å has two components, one propagating perpendicular and another along (parallel to) the flare region. While the parallel propagating component gets reflected backward from the other leg of the flare loops (Figure 2a and 2c), the perpendicular component freely propagates outward. After 09:32 UT, a rising filament can be seen above the active region. The EUV wave is also observed in AIA 211 Å and AIA 193 Å. In the AIA 211 Å images, it is observed as a freely propagating outward moving structure (Figure 2d).

After checking the coronagraph images, it was found that the eruption is accompanied by a CME. The evolution of the CME observed by STEREO-B/SECCHI-EUVI, STEREO-B/SECCHI-COR1, and SOHO/LASCO is shown in Figure 3. The earliest signature and evolution of the CME revealed in EUV wavelength by STEREO-B/SECCHI-EUVI 195 Å running difference images at 09:26 UT, 09:31 UT, and 09:36 UT are presented in Figures 3b–d, showing a slow evolution of the loop system, which started at the impulsive phase of the flare.
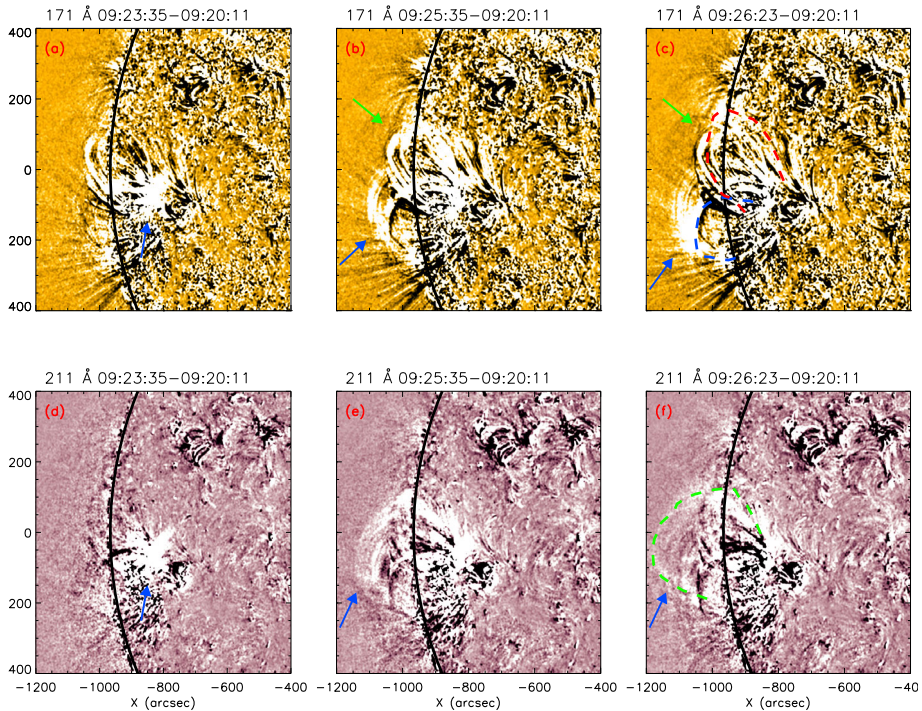
Figure 2 (a–c) Base difference images at AIA 171 Å showing the evolution of EUV wave components moving parallel (blue arrow) and perpendicular (green arrow) from the active region. (d–f) Base difference images at AIA 211 Å showing the outward moving EUV wave structure indicated by green curve (blue arrow). An animation of the AIA images is available.

The CME is observed at STEREO-B/SECCHI-EUVI at the same time when the EUV wave is at the edge of AIA FOV. The AIA instruments and the twin STEREO spacecraft observations were compared and found that the CME loop structure is moving ahead and independent of the observed EUV wave. Further in STEREO-B/SECCHI-COR1 FOV, the expanding loop structure is visible at 09:36 UT. The expanding structure, probably the CME, will take several minutes to reach the SOHO/LASCO-C2 FOV at heights $> 2.2\ R_\odot$. Therefore the structure is visible in the SOHO/LASCO-C2 FOV at 10:12 UT. This observation clearly shows that the eruption is accompanied by a CME, whereas the previous authors (Kumar and Innes, 2015) had missed it, likely due to not including STEREO/SECCHI observations in their analysis. They claimed that there was no CME loop behind the EUV wave.

3.2. Radio Imaging

The NRH provides radio imaging at nine different frequencies from $450 – 150$ MHz. Highly sensitive NRH imaging observations were used to find the temporal position and outward motion of radio sources from the eruptive site. They can also be utilized to identify the onset of radio emissions or high-frequency counterpart of the radio emissions, which are possibly not recorded in the dynamic spectrum due to low instrument resolution. The present study utilized the NRH imaging data with temporal resolution of 0.25 s. The total radio flux profiles recorded at 270, 228, 173, and 150 MHz were plotted over the dynamic spectrum
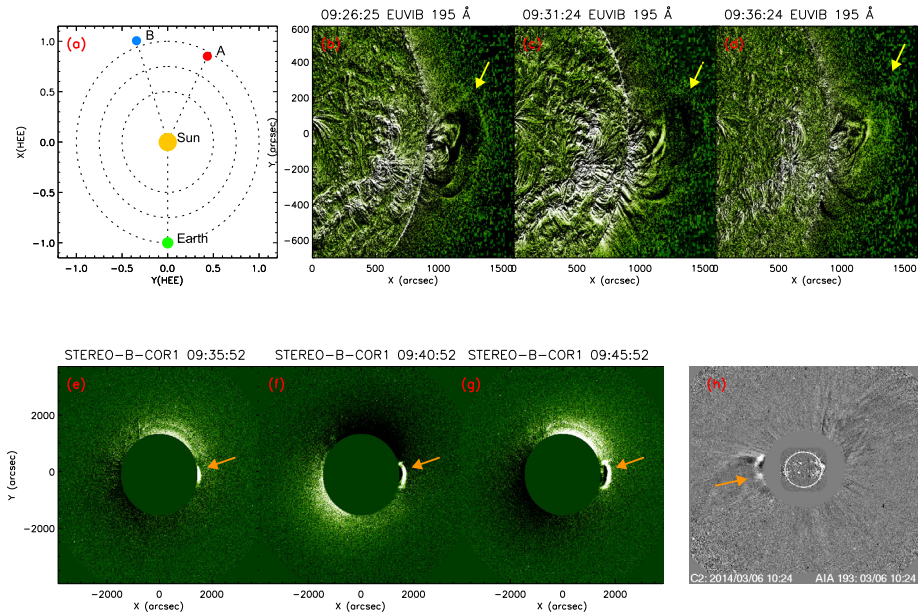
Figure 3 (a) Spacecraft locations (A and B denote the STEREO spacecraft positions, Sun denotes the Sun, Earth denotes the ground based observations (metric radio wavelengths). (b–d) Snapshot of STEREO-B/SECCHI-EUVI running difference images at 195 Å showing the eruptive structures (see yellow arrow). (e–h) The temporal and structural evolution of the CME by STEREO-B/SECCHI-COR1 at 09:35 UT, 09:40 UT, and 09:45 UT and SOHO/LASCO-C2 at 10:24 UT (orange arrow). An animation of the STEREO-B/SECCHI-EUVI running difference images is available.

in Figure 1a as colored curves to identify the onset of the type II burst. The evolution of the dominant source is compared with radio features in the radio dynamic spectrum. The radio sources are identifiable only for the harmonic band due to the instrumental limit, i.e., the last observable NRH radio imaging observations. Using the Nançay radio imaging data, different kinds of radio bursts can be easily identified by their shifts of the total flux maximum at subsequent frequencies with time. The total flux data observed by NRH single frequencies are consistent with the type III and type II bursts in the dynamic spectrum.

Figure 4 shows the temporal evolution of radio sources at different NRH frequencies: 228, 173 and 150 MHz. An accompanying animation is provided as electronic supplementary material to show the temporal and spatial evolutions of the emissions at the six NRH frequencies between 327 and 150 MHz. The contours represent the 95% and 90% levels of the T_{Bmax}. In the animation, we see that before the type III burst, the AR released weak radio emissions with $T_{\mathrm{Bmax}} = 10^6$ K. The type III radio burst starts at 09:23:05 UT, attains the T_{Bmax} of 10^6 K at 09:23:20 UT, and ends at 09:24:10 UT.

The type II burst first appeared in the NRH FOV at 09:25:50 UT at 228 MHz. Later on, it appeared at successively lower frequencies. At 173 MHz, the T_{Bmax} is 4.5×10^{10} K at 09:27:39 UT, whereas it is 10^9 K at 09:27:05 UT at 228 MHz, and also at 09:29:07 UT at 150 MHz. The T_{Bmax} reaches higher values at lower frequencies. The type II sources can be identified from 228 MHz to lower-frequency channels one after the other with some delay consistent with the drifting motion from higher to lower frequencies observed in the radio dynamic spectrum. The radio sources disappearing at high altitude indicate that the type II emission had either ceased or moved out of the NRH FOV.
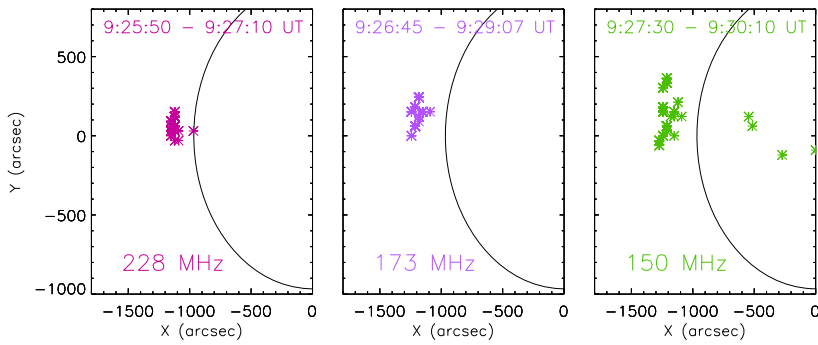
Figure 4 Temporal evolution of radio source centers from NRH images at different frequencies. An animation of the NRH radio imaging at different frequencies is available.
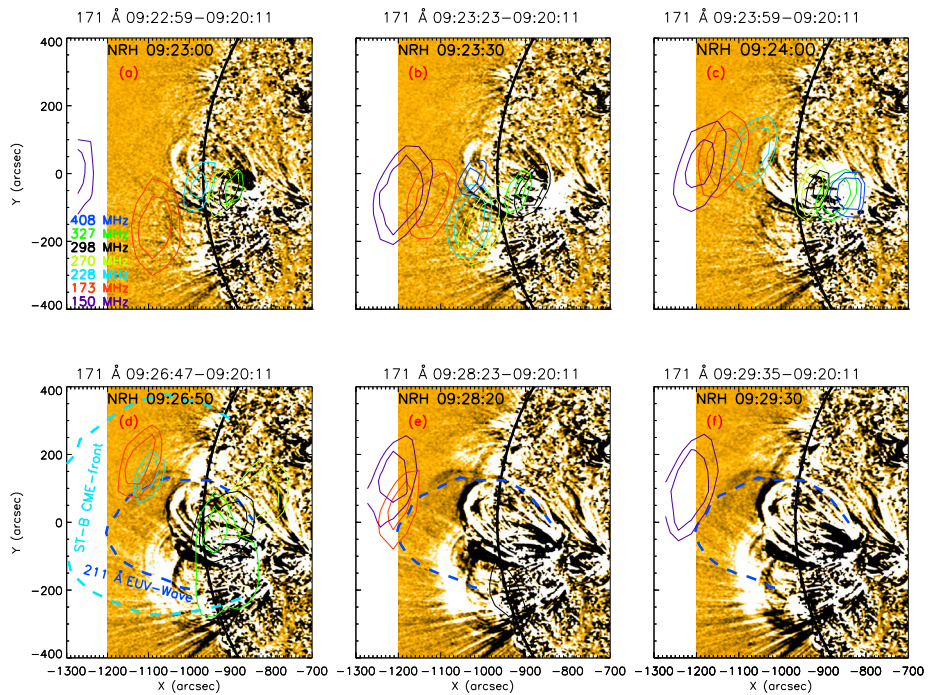

Figure 5 Temporal evolution of NRH sources superposed on the closest-in-time of AIA 171 Å images, the blue curve presents the EUV wave observed at AIA 211 Å image, and cyan color curve represents the CME frontal structure observed in the STEREO-B/SECCHI-EUVI closest-in-time image. The upper row of images shows the type III burst locations to verify the frequency–height dependence on plasma emission, and the lower row shows the type II burst. The NRH data are represented by the $90-95\%$ T_{Bmax} contour. An animation of this figure is available.

In Figure 5 the NRH sources from $408-150$ MHz were plotted over the temporally closest SDO/AIA 171 Å images to examine the temporal and spatial evolutions of radio emission relative to the eruptive structures. The line-up of type III radio sources from higher to lower frequencies simultaneously at all frequency channels implies the propagation of
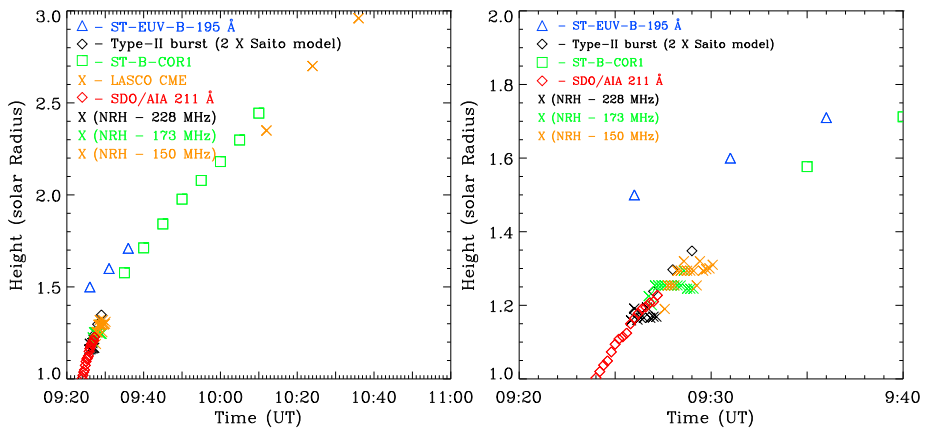
Figure 6 Kinematics of the EUV wave and CME structures with metric type II shock signatures.

electron beam along open-field or large-scale loop structure (Ginzburg and Zhelezniakov 1958; Melrose 1980). Energetic electrons are usually believed to be accelerated by magnetic reconnection in solar flares. In the case of type II radio burst, the observed NRH data show the shift of radio sources from higher to lower frequencies with time. The type II radio sources at 173 and 150 MHz, located at the flank of the EUV wave observed in the AIA 211 Å channel presented by dotted blue line in Figure 5d–f, indicate the presence of a shock. In the STEREO-B/SECCHI-EUVI image, the radio sources are located at lower heights than the frontal eruptive structure. This height difference between the CME leading edge and the shock wave implies that the type II burst is not driven by the CME bow shock.

The NRH has imaged the type II burst only in the second harmonic emission. It is important to note that the radio sources corresponding to harmonic and fundamental bands will appear close to each other. Yet their sources may look different due to refraction and scattering. The radio source corresponding to the fundamental band might be twice larger in size than its harmonic counterpart. The shift in position of the radio source due to iono-spheric refraction is $< 0.1\ R_{\odot}$ at 160 MHz. Therefore the refraction effects will be minimal at higher frequencies (for details, see Stewart and McClean, 1982). The error in estimating the type II burst location is $0.08 - 0.2\ R_{\odot}$ and is due to the angular resolution of the NRH observations.

In the case of piston driven shock, the shock wave will propagate ahead of the CME. If the situation is such that the shock wave is produced at the CME flank and not on the CME front, then the height of the shock structure will be smaller than the height of CME front. So the possibility of shock being on the CME flank is unlikely. Furthermore, it is important to note that for the case of CME-driven shock (bow shock), the CME speed would be close to the speed of shock wave. In contrast, the CME has a speed of ~ 280 km s^{-1}, and type II speed is ~ 650 km s^{-1}, which implies that the CME was probably not driving the shock wave. Thus it is concluded that CME might not be the driver of shock wave in the present case.

3.3. Kinematic Evolution

Figure 6 shows the kinematics of radio emission and the eruptive structure observed between $09:20 - 11:20$ UT across multitude wavelength radio, EUV, and white-light observations from different instruments. The height–time plots from STEREO-B/SECCHI-EUVI,

STEREO-B/SECCHI-COR1, and SOHO/LASCO-C2 show that the same feature is continuously tracked across different instruments. The EUV wave from SDO/AIA at 211 Å observed between 09:24 – 09:27 UT is located at $1.003 - 1.22 \ R_\odot$ and the radio sources at different NRH frequencies, i.e., 228 MHz radio sources are located between $1.16 \ R_\odot$ at 09:26 UT to $1.19 \ R_\odot$ at 09:27 UT, 173 MHz radio sources are located between $1.20 \ R_\odot$ at 09:27 UT to $1.25 \ R_\odot$ at 09:29 UT, and 150 MHz radio sources are located between $1.25 \ R_\odot$ at 09:28 UT to $1.32 \ R_\odot$ at 09:30 UT. Therefore the EUV wave from SDO/AIA at 211 Å and type II radio burst imaged by NRH were synchronized, indicating the flare shock as a possible factor for the origin of radio emission. The measured speed of CME was in the range $252 - 280$ km s^{-1}, and such slow CME might not be able to drive a shock. On the other hand, the flare-triggered fast mode wave could lead to the shock wave as it propagates at a speed of ~ 820 km s^{-1}. The radio measurements from the dynamic spectra and employing the $2\times$ Saito density model corresponds to the height of $1.18 \ R_\odot$ at 09:26 UT to $1.35 \ R_\odot$ at 09:29 UT; further, the height–time measurements yield a speed of ~ 650 km s^{-1}. This also indicates that the type II radio emission in the present case might be excited by the flare shock and not by the CME.

The rising loop-like feature observed by STEREO-B/SECCHI-EUVI is the earliest possible CME leading-edge observation detected between $1.5 - 1.71 \ R_\odot$, thereafter continuously observed by STEREO-B/SECCHI-COR1 between $1.58 - 2.44 \ R_\odot$, and later in the SOHO/LASCO-C2 FOV from $2.35 - 4.15 \ R_\odot$. This shows that the high-located EUV loops started to move outward and the EUV wave from behind created the type II burst and probably made the lower-located CME materials to move faster. The impulsive flare triggered the fast-moving EUV wave. The height–time measurements from the dynamic spectrum and the type II sources imaged by NRH observations at 228, 173, and 150 MHz synchronized with each other indicate the flare shock as a possible factor for the origin of type II radio burst. Also cannot rule out the possibility that both the flare and CME might contribute to the shock wave. However, in the present case the observational evidence supports the flare shock scenario.

4. Discussion

The present study provides a strong evidence of EUV wave being a MHD shock that excited the metric type II radio burst. The type II radio burst is observed by three NRH frequencies at 228, 173, and 150 MHz, which enables tracking the outward motion of harmonic band radio sources. The NRH radio sources were located at the flank of the EUV wave observed in the AIA 171 Å and AIA 211 Å channels. There is a weak CME observed in STEREO-B/SECCHI-COR1 and SOHO/LASCO images.

The origin of coronal shocks that generate type II radio bursts is still under debate. Most of the observed type II radio bursts were accompanied by CMEs and are usually considered as shock drivers. In the event presented herein, the EUV wave and the associated shock were seemingly triggered by the flare energy release. The radio sources located at the flank of the EUV wave evidences that the EUV wave acts as the source of the radio emission. STEREO observed the CME in STEREO-B/SECCHI-EUVI and SECCHI-COR1 images. Overplotting the NRH sources and the heights of eruptive structure in STEREO-B/SECCHI-EUVI on the AIA 171 Å images show that radio sources are associated with the EUV wave and not with the CME leading edge. This indicates that the shock is probably ignited by the flare. Similarly, Wagner and MacQueen (1983) found in one event recorded by Culgoora Radio Heliograph data that the radio source was located well below the white-light transient

before the event has reached the height of 2 $R_{\odot}$ and the shock was considerably faster than the CME. Thus they concluded that the type II radio burst is independent of the CME and a shock might be ignited by the associated flare. A similar conclusion was also reported by Vršnak et al. (2006) using NRH data.

There are few case studies recently reported either without CME or with a slow CME maintains the debate on the origin of coronal shocks (Magdalenić et al., 2012; Su et al., 2015; Eselevich et al., 2017) whether flare or CME acts as a driver for their generation. We have to explore the context in detail in future studies. It is important to note that even now with high-resolution imaging observations from SDO/AIA, we still lack the observation of low coronal features for CMEs without bright fronts.

5. Conclusions

Using combined data analysis, the detailed case study of a metric type II radio burst, which occurred on 06 March 2014 accompanied by an impulsive flare, and a CME is reported. It is a classical radio event that contains type III and type II radio bursts. The type II radio burst is observed with both fundamental and harmonic structures in the frequency range of 235–130 MHz (120–60 MHz) in harmonic (fundamental) bands with a life time of 5 min between 09:26–09:31 UT. The estimated speed of the type II radio burst by employing the $2\times$ Saito electron density model is found to be ~ 650 km s^{-1}.

The type II radio burst is related to a coronal EUV wave clearly identified in AIA 171, 211, and 193 Å images. AIA 171 and 211 Å images were used to show the wave evolution. At AIA 171 Å, it has two components, one propagating parallel and other propagating perpendicular to the flare site. The parallel component gets reflected backward from one of the flare loops, and the perpendicular component freely propagates outward. The wave is also observed in AIA 211 Å images as a freely propagating outward moving structure. The estimated speed of the EUV wave at AIA 171 Å is ~ 820 km s^{-1}.

The source position of the type II radio burst is observed at 228, 173, and 150 MHz NRH imaging frequencies. The NRH radio sources superposed on the AIA 171 Å images reveal that the radio burst is excited at the outward moving EUV wave. The eruption is also accompanied by a weak CME observed with a sky plane speed of ~ 252 km s^{-1} in the SOHO/LASCO-C2 FOV and ~ 280 km s^{-1} in the STEREO-B/SECCHI-COR1 FOV. The difference in speed between CME and type II burst implies that CME was probably not driving the shock. The height–time plots of the type II burst and eruptive structures at different wavelengths show that the high-located EUV loops started to move outward and the EUV wave from behind created the type II burst and probably made the lower CME-materials to move faster. The flare energy release and the onset of EUV wave occurred simultaneously, as well as the speed between the EUV wave and type II burst lies closer to each other. Therefore the observed type II radio burst and the EUV wave are probably ignited by the flare.

Author contributions   V. V analysed the event, prepared the figures and animations, wrote as well as reviewed and revised the manuscript.

Data Availability   No datasets were generated or analysed during the current study.

Declarations

Competing interests   The authors declare no competing interests.

References

Bougeret, J.-L., Kaiser, M.L., Kellogg, P.J., Manning, R., Goetz, K., Monson, S.J., Monge, N., Friel, L., Meetre, C.A., Perche, C., Sitruk, L., Hoang, S.: 1995, Waves: the radio and plasma wave investigation on the wind spacecraft. *Space Sci. Rev.* **71**(1–4), 231. DOI. ADS.

Bougeret, J.L., Goetz, K., Kaiser, M.L., Bale, S.D., Kellogg, P.J., Maksimovic, M., Monge, N., Monson, S.J., Astier, P.L., Davy, S., Dekkali, M., Hinze, J.J., Manning, R.E., Aguilar-Rodriguez, E., Bonnin, X., Briand, C., Cairns, I.H., Cattell, C.A., Cecconi, B., Eastwood, J., Ergun, R.E., Fainberg, J., Hoang, S., Huttunen, K.E.J., Krucker, S., Lecacheux, A., MacDowall, R.J., Macher, W., Mangeney, A., Meetre, C.A., Moussas, X., Nguyen, Q.N., Oswald, T.H., Pulupa, M., Reiner, M.J., Robinson, P.A., Rucker, H., Salem, C., Santolik, O., Silvis, J.M., Ullrich, R., Zarka, P., Zouganelis, I. (eds.): 2008, S/WAVES: the radio and plasma wave investigation on the STEREO mission. *Space Sci. Rev.* **136**(1–4), 487. DOI. ADS.

Brueckner, G.E., Howard, R.A., Koomen, M.J., Korendyke, C.M., Michels, D.J., Moses, J.D., Socker, D.G., Dere, K.P., Lamy, P.L., Llebaria, A., Bout, M.V., Schwenn, R., Simnett, G.M., Bedford, D.K., Eyles, C.J.: 1995, The Large Angle Spectroscopic Coronagraph (LASCO). *Solar Phys.* **162**, 357. DOI. ADS.

Chen, Y., Du, G., Feng, L., et al.: 2014, *Astrophys. J.* **787**, 59. DOI.

Domingo, V., Fleck, B., Poland, A.I.: 1995, The SOHO mission: an overview. *Solar Phys.* **162**, 1. DOI. ADS.

Dulk, G.A.: 1985, Radio emission from the sun and stars. *Annu. Rev. Astron. Astrophys.* **23**, 169. DOI. ADS.

Eselevich, V.G., Eselevich, M.V., Zimovets, I.V., Sharykin, I.N.: 2017, Evidence for shock generation in the solar corona in the absence of coronal mass ejections. *Astron. Rep.* **61**, 805. DOI. ADS.

Feng, S.W., Chen, Y., Kong, X.L., et al.: 2013, *Astrophys. J.* **767**, 29. DOI.

Gopalswamy, N., Lara, A., Kaiser, M.L., Bougeret, J.-L.: 2001, Near-Sun and near-Earth manifestations of solar eruptions. *J. Geophys. Res.* **106**, 25261. DOI. ADS.

Kaiser, M.L., Kucera, T.A., Davila, J.M., St. Cyr, O.C., Guhathakurta, M., Christian, E.: 2008, The STEREO mission: an introduction. *Space Sci. Rev.* **136**, 5. DOI. ADS.

Kerdraon, A., Delouis, J.-M.: 1997, The Nançay Radioheliograph. In: Trottet, G. (ed.) *Coronal Physics from Radio and Space Observations, Lecture Notes in Physics, Berlin Springer Verlag* **483**, 192. DOI. ADS.

Kong, X.L., Chen, Y., Li, G., et al.: 2012, *Astrophys. J.* **750**, 158. DOI.

Kumar, P., Innes, D.E.: 2015, Partial reflection and trapping of a fast-mode wave in solar coronal arcade loops. *Astrophys. J. Lett.* **803**, L23. DOI. ADS.

Kumar, P., Innes, D.E., Cho, K.-S.: 2016, Flare-generated shock wave propagation through solar coronal arcade loops and an associated type II radio burst. *Astrophys. J.* **828**, 28. DOI. ADS.

Kumar, P., Cho, K.-S., Chen, P.F., Bong, S.-C., Park, S.-H.: 2013, Multiwavelength study of a solar eruption from AR NOAA 11112: II. Large-scale coronal wave and loop oscillation. *Solar Phys.* **282**, 523. DOI. ADS.

Lara, A., Gopalswamy, N., Nunes, S., Muñoz, G., Yashiro, S.: 2003, A statistical study of CMEs associated with metric type II bursts. *Geophys. Res. Lett.* **30**, 8016. DOI. ADS.

Lemen, J.R., Title, A.M., Akin, D.J., Boerner, P.F., Chou, C., Drake, J.F., Duncan, D.W., Edwards, C.G., Friedlaender, F.M., Heyman, G.F., Hurlburt, N.E., Katz, N.L., Kushner, G.D., Levay, M., Lindgren, R.W., Mathur, D.P., McFeaters, E.L., Mitchell, S., Rehse, R.A., Schrijver, C.J., Springer, L.A., Stern, R.A., Tarbell, T.D., Wuelser, J.-P., Wolfson, C.J., Yanari, C., Bookbinder, J.A., Cheimets, P.N., Caldwell, D., Deluca, E.E., Gates, R., Golub, L., Park, S., Podgorski, W.A., Bush, R.I., Scherrer, P.H., Gummin, M.A., Smith, P., Auker, G., Jerram, P., Pool, P., Soufli, R., Windt, D.L., Beardsley, S., Clapp, M., Lang, J., Waltham, N.: 2012, The Atmospheric Imaging Assembly (AIA) on the Solar Dynamics Observatory (SDO). *Solar Phys.* **275**, 17. DOI. ADS.

Lin, R.P., Dennis, B.R., Hurford, G.J., Smith, D.M., Zehnder, A., Harvey, P.R., Curtis, D.W., Pankow, D., Turin, P., Bester, M., Csillaghy, A., Lewis, M., Madden, N., van Beek, H.F., Appleby, M., Raudorf, T., McTiernan, J., Ramaty, R., Schmahl, E., Schwartz, R., Krucker, S., Abiad, R., Quinn, T., Berg, P., Hashii, M., Sterling, R., Jackson, R., Pratt, R., Campbell, R.D., Malone, D., Landis, D., Barrington-Leigh, C.P., Slassi-Sennou, S., Cork, C., Clark, D., Amato, D., Orwig, L., Boyle, R., Banks, I.S., Shirey, K., Tolbert, A.K., Zarro, D., Snow, F., Thomsen, K., Henneck, R., McHedlishvili, A., Ming, P., Fivian, M., Jordan, J., Wanner, R., Crubb, J., Preble, J. (eds.): 2002, The Reuven Ramaty High-Energy Solar Spectroscopic Imager (RHESSI). *Solar Phys.* **210**, 3. DOI. ADS.

Long, D.M., Bloomfield, D.S., Chen, P.F., Downs, C., Gallagher, P.T., Kwon, R.-Y., Vanninathan, K., Veronig, A.M., Vourlidas, A., Vršnak, B., Warmuth, A., Žic, T.: 2017, Understanding the physical nature of coronal "EIT waves". *Solar Phys.* **292**, 7. DOI. ADS.

Magdalenić, J., Vršnak, B., Pohjolainen, S., Temmer, M., Aurass, H., Lehtinen, N.J.: 2008, A flare-generated shock during a coronal mass ejection on 24 December 1996. *Solar Phys.* **253**, 305. DOI. ADS.

Magdalenić, J., Marqué, C., Zhukov, A.N., Vršnak, B., Žic, T.: 2010, Origin of coronal shock waves associated with slow coronal mass ejections. *Astrophys. J.* **718**, 266. DOI. ADS.

Magdalenić, J., Marqué, C., Zhukov, A.N., Vršnak, B., Veronig, A.: 2012, Flare-generated type II burst without associated coronal mass ejection. *Astrophys. J.* **746**, 152. DOI. ADS.

Maričić, D., Vršnak, B., Stanger, A.L., Veronig, A.M., Temmer, M., Roša, D.: 2007, Acceleration phase of coronal mass ejections: II. Synchronization of the energy release in the associated flare. *Solar Phys.* **241**, 99. DOI. ADS.

McLean, D.J., Labrum, N.R.: 1985, Solar radiophysics: Studies of emission from the Sun at metre wavelengths. ADS.

Nelson, G.J., Melrose, D.B.: 1985, In: McLean, D.J., Labrum, N.R. (eds.) *Type II Bursts*, 333. ADS.

Payne-Scott, R., Yabsley, D.E., Bolton, J.G.: 1947, Relative times of arrival of bursts of solar noise on different radio frequencies. *Nature* **160**, 256. DOI. ADS.

Pesnell, W.D., Thompson, B.J., Chamberlin, P.C.: 2012, The Solar Dynamics Observatory (SDO). *Solar Phys.* **275**, 3. DOI. ADS.

Pohjolainen, S., Lehtinen, N.J.: 2006, Slow halo CMEs with shock signatures. *Astron. Astrophys.* **449**, 359. DOI. ADS.

Prakash, O., Umapathy, S., Shanmugaraju, A., Vasanth, V.: 2012, Kinematics and flare properties of radio-loud CMEs. *Solar Phys.* **281**, 765. DOI. ADS.

Reames, D.V.: 1999, Particle acceleration at the Sun and in the heliosphere. *Space Sci. Rev.* **90**, 413. DOI. ADS.

Saito, K., Makita, M., Nishi, K., Hata, S.: 1970, A non-spherical axisymmetric model of the solar K corona of the minimum type. *Ann. Tokyo Astron. Obs.* **12**, 53. ADS.

Shanmugaraju, A., Suresh, K., Vasanth, V., Selvarani, G., Umapathy, S.: 2018, Interplanetary type II radio bursts and their association with CMEs and flares. *Astrophys. Space Sci.* **363**, 126. DOI. ADS.

Su, W., Cheng, X., Ding, M.D., Chen, P.F., Sun, J.Q.: 2015, A type II radio burst without a coronal mass ejection. *Astrophys. J.* **804**, 88. DOI. ADS.

Temmer, M., Veronig, A.M., Kontar, E.P., Krucker, S., Vršnak, B.: 2010, Combined STEREO/RHESSI study of coronal mass ejection acceleration and particle acceleration in solar flares. *Astrophys. J.* **712**, 1410. DOI. ADS.

Thompson, B.J., Gurman, J.B., Neupert, W.M., Newmark, J.S., Delaboudinière, J.-P., Cyr, O.C.S., Stezelberger, S., Dere, K.P., Howard, R.A., Michels, D.J.: 1999, SOHO/EIT observations of the 1997 April 7 coronal transient: possible evidence of coronal moreton waves. *Astrophys. J. Lett.* **517**, L151. DOI. ADS.

Vasanth, V., Umapathy, S.: 2013a, A statistical study on CMEs associated with DH-type-II radio bursts based on their source location (limb and disk events). *Solar Phys.* **282**, 239. DOI. ADS.

Vasanth, V., Umapathy, S.: 2013b, A statistical study on DH CMEs and its geoeffectiveness. *ISRN Astron. Astrophys.* **2013**, 1. DOI. ADS.

Vasanth, V., Umapathy, S., Vršnak, B., Anna Lakshmi, M.: 2011, Characteristics of type-II radio bursts associated with flares and CMEs. *Solar Phys.* **273**, 143. DOI. ADS.

Vasanth, V., Umapathy, S., Vršnak, B., Žic, T., Prakash, O.: 2014, Investigation of the coronal magnetic field using a type II solar radio burst. *Solar Phys.* **289**, 251. DOI. ADS.

Vasanth, V., Chen, Y., Kong, X.L., Wang, B.: 2015, Investigation of the geoeffectiveness of CMEs associated with IP type II radio bursts. *Solar Phys.* **290**, 1815. DOI. ADS.

Vršnak, B.: 2001, Solar flares and coronal shock waves. *J. Geophys. Res.* **106**, 25291. DOI. ADS.

Vršnak, B., Cliver, E.W.: 2008, Origin of coronal shock waves. Invited review. *Solar Phys.* **253**, 215. DOI. ADS.

Vršnak, B., Lulić, S.: 2000, Formation of coronal MHD shock waves – II. The pressure pulse mechanism. *Solar Phys.* **196**, 181. DOI. ADS.

Vršnak, B., Warmuth, A., Brajša, R., Hanslmeier, A.: 2002, Flare waves observed in Helium I 10 830 Å. A link between Hα Moreton and EIT waves. *Astron. Astrophys.* **394**, 299. DOI. ADS.

Vršnak, B., Maričić, D., Stanger, A.L., Veronig, A.: 2004, Coronal mass ejection of 15 may 2001: II. Coupling of the CME acceleration and the flare energy release. *Solar Phys.* **225**, 355. DOI. ADS.

Vršnak, B., Warmuth, A., Temmer, M., Veronig, A., Magdalenić, J., Hillaris, A., Karlický, M.: 2006, Multi-wavelength study of coronal waves associated with the CME-flare event of 3 November 2003. *Astron. Astrophys.* **448**, 739. DOI. ADS.

Wagner, W.J., MacQueen, R.M.: 1983, The excitation of type II radio bursts in the corona. *Astron. Astrophys.* **120**, 136. ADS.

Wild, J.P., McCready, L.L.: 1950, Observations of the spectrum of high-intensity solar radiation at metre wavelengths. I. The apparatus and spectral types of solar burst observed. *Aust. J. Sci. Res., Ser. A* **3**, 387. DOI. ADS.

Wu, S.T., Zheng, H., Wang, S., Thompson, B.J., Plunkett, S.P., Zhao, X.P., Dryer, M.: 2001, Three-dimensional numerical simulation of MHD waves observed by the extreme ultraviolet imaging telescope. *J. Geophys. Res.* **106**, 25089. DOI. ADS.

Zhang, J., Dere, K.P., Howard, R.A., Kundu, M.R., White, S.M.: 2001, On the temporal relationship between coronal mass ejections and flares. *Astrophys. J.* **559**, 452. DOI. ADS.

Zhang, J., Dere, K.P., Howard, R.A., Vourlidas, A.: 2004, A study of the kinematic evolution of coronal mass ejections. *Astrophys. J.* **604**, 420. DOI. ADS.